Substrate binding and carboxylation by dethiobiotin synthetase — a kinetic and X-ray study

Dmitriy Alexeev[1], Robert L Baxter[2]*, Otto Smekal[2] and Lindsay Sawyer[1]*

[1]Department of Biochemistry, The University of Edinburgh, Hugh Robson Building, George Square, Edinburgh EH8 9XD, UK and [2]Department of Chemistry, The University of Edinburgh, King's Buildings, West Mains Road, Edinburgh EH9 3JJ, UK

Background: The vitamin biotin is a ubiquitous prosthetic group of carboxylase and transcarboxylase enzymes. Biotin biosynthesis occurs by similar pathways in microorganisms and plants. The penultimate step in biotin biosynthesis, catalyzed by dethiobiotin synthetase (DTBS), involves a unique ATP-dependent *N*-carboxylation, resulting in formation of the *ureido* ring function of dethiobiotin. The first two steps of dethiobiotin formation, which is a complex, multistep enzymatic reaction, have been elucidated by a combination of X-ray crystallography and kinetic methods.

Results: The first step in catalysis by DTBS is the formation of an enzyme–substrate complex and the second is the enzymatic carboxylation of the bound substrate. Both steps are Mg^{2+} dependent. The kinetic constants in the presence and absence of Mg^{2+} have been measured and a set of X-ray structures determined at different stages of the reaction. The conformational changes in the active site of the enzyme, induced by Mg^{2+}, substrate binding and substrate carboxylation, have been monitored crystallographically and are discussed. Sulfate ions bound to DTBS may mimic the behaviour of the α- and γ-phosphates of ATP in Mg^{2+} binding and in the subsequent steps of the reaction.

Conclusions: Mg^{2+} is an essential cation for both substrate binding and carbamate formation by DTBS, when sulfate is present. The conformational changes induced at the active site in the DTBS–substrate complex, when Mg^{2+} is present, are small yet highly significant and serve to optimize the interactions between substrate and enzyme. DTBS is active as a homodimer and the substrate-binding site straddles both monomers in the dimer. The carboxylation site is unambiguously identified as the N-7 amino group of the substrate, rather than the N-8 amino group, as previously suggested. The elongated nucleotide-binding loop (the P loop) binds both ATP and substrate in a manner which suggests that this feature may be of wider importance.

Structure 15 November 1995, **3**:1207–1215

Key words: carbamate intermediate, carboxylation, dethiobiotin synthetase, diaminopelargonic acid

Introduction

Determining the sequence of events that occurs during an enzyme-catalyzed reaction requires painstaking chemical and kinetic studies (see [1]), even when the reaction is a 'simple' one- or two-step process. With complex multistep reactions, kinetic resolution of the individual steps becomes increasingly more difficult, although, in contrast, chemical and crystallographic distinction of intermediates may become easier. Indeed, under the right conditions it may be possible, using spectroscopic and crystallographic methods, to define the structures of intermediates at various steps in a reaction sequence, enabling verification of a proposed mechanism. In this paper we report the results of spectroscopic and crystallographic studies on the first two steps of the complex reaction catalyzed by *Escherichia coli* dethiobiotin synthetase (DTBS, E.C. 6.3.3.3), an ATP-dependent carboxylase.

The vitamin biotin, which is the cofactor in most biological carboxylation and transcarboxylase reactions, is synthesized by what now appears to be a common route for both microorganisms and plants. [2–6]. The penultimate step in the biotin biosynthetic pathway is catalyzed by DTBS and involves the conversion of the *erythro* diamine of (7*R*,8*S*) 7,8-diaminononanoic acid (7,8-diaminopelargonate or DAPA, structure 1, Fig. 1) to the *ureido* ring function of dethiobiotin (DTB, structure 2, Fig. 1) [7,8]. This ATP-dependent reaction, shown in Figure 1, requires CO_2 as the CO donor, thus placing DTBS among the small group of carboxylating enzymes that use CO_2 rather than the hydrogen carbonate anion. A tenuous connection, based solely on the role of CO_2 as a substrate, can thus be made between DTBS and both ribulose-1,5-bisphosphate carboxylase/oxidase and Mn^{2+}-dependent pyruvate carboxylase [9,10].

We have cloned the *E. coli* enzyme encoded by the bioD gene into a modified pBR322 plasmid, overexpressed the gene and purified the protein [11]. This enabled us to carry out a series of chemical, kinetic and crystallographic studies [12–14] that have established the sequence of chemical reactions involved in the formation of DTB from DAPA. Our initial assignment of the structure of the first enzyme-bound intermediate as the N-8 rather than the N-7 substituted carbamate (i.e. species 4 rather than 3, Fig. 1) followed from the results of a trapping experiment in which the enzyme–DAPA–$^{14}CO_2$ complex was freeze dried and methylated, resulting in a dimethyl ester of the carbamate species [12]. An obvious criticism of this experiment, that now seems quite valid, is that water abstraction results in changes in the carbamate binding, allowing equilibration to give the thermodynamically more stable N-8 carbamate. In the enzyme action, the intermediate carbamate is subsequently phosphorylated

*Corresponding authors.

 ISSN 0969-2126

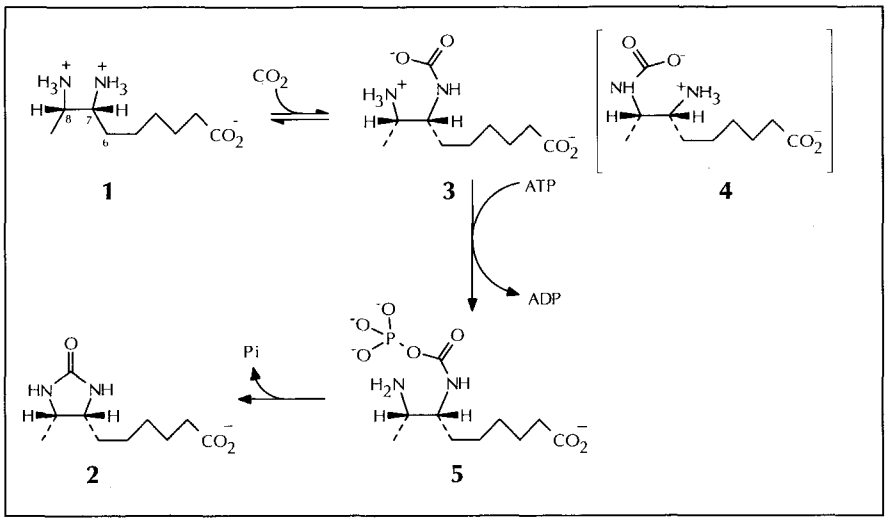

Fig. 1. The sequence of reactions catalyzed by dethiobiotin synthetase (DTBS).

by ATP, to give a mixed anhydride (structure 5, Fig. 1) anhydride 5. The *ureido* ring of the product is then generated as the result of nucleophilic attack of the vicinal amino group, with release of inorganic phosphate [13].

The crystal structure of the enzyme has been determined in this laboratory [14], at 1.8 Å resolution, and independently by Huang *et al.* [15]. We identified the location of the DAPA- and ATP-binding sites on the enzyme, but without details of the interaction between the DAPA molecule and the protein. Here we report spectroscopic and crystallographic characterization of the enzyme–DAPA and enzyme–DAPA.CO_2 (DAPA carbamate) complexes, in the presence and absence of Mg^{2+} ions, that reveal, in detail, the specific protein–substrate and protein–intermediate interactions that stabilize the binding of DAPA and the DAPA N-7 carbamate to the active site of the enzyme.

Results and discussion

General outline of the experiments

The first two steps of the reaction catalyzed by DTBS involve the binding of DAPA to the enzyme and the subsequent reaction of this complex with CO_2, resulting in a DTBS–DAPA.CO_2 complex. This is schematically presented in Figure 2. Evidence that this is a realistic model follows both from trapping experiments (RL Baxter *et al.*, unpublished data) and the observation of absorption changes in the UV spectrum of DTBS following DAPA binding and reaction of CO_2 with the complex. Principal component analysis of raw spectroscopic data reveals two intermediate species, with absorption maxima at 290±4 nm and 301±3 nm, corresponding to the DTBS–DAPA and DTBS–DAPA.CO_2 complexes. The

$$\text{DAPA + DTBS} \underset{k_{-1}}{\overset{k_1}{\rightleftharpoons}} \text{DTBS-DAPA + } CO_2 \underset{k_{-2}}{\overset{k_2}{\rightleftharpoons}} \text{DTBS-DAPA.}CO_2$$

Fig. 2. Kinetic model for the first two steps of the DTBS reaction in the absence of ATP.

second species was not detected in the absence of CO_2. We used these absorption changes to measure the kinetic constants of the reaction with and without Mg^{2+}. The components of the reaction (DAPA, CO_2, Mg^{2+}) were soaked into crystals of DTBS and the crystal structures were determined, providing 'snapshots' of the structural changes at various stages of the reaction. The combination of the kinetic and structural data allows us to analyze the reaction mechanism in detail.

Details of the X-ray data sets collected from crystals of DTBS soaked under various conditions are shown in Tables 1 and 2. Data set N_2–DAPA–Mg^{2+} was collected from a soak prepared in buffer supplemented with 20 mM Mg^{2+} and equilibrated in a CO_2-free nitrogen atmosphere under which, on the basis of solution spectroscopic data, the substrate is definitely not carboxylated. Data set CO_2–DAPA–Mg^{2+} was collected from the same crystal equilibrated in a CO_2 atmosphere, where we expected the substrate to be *N*-carboxylated. The third data set was obtained from a crystal soaked in buffer containing no Mg^{2+}, under a normal air atmosphere. These last conditions correspond to the solution experiment in which we observe DAPA binding to the enzyme but no carbamate formation. The kinetic constants k_1, k_{-1}, k_2 and k_{-2} (see Fig. 2) were determined.

Both steps of the reaction are Mg^{2+}-dependent

In the absence of cooperative interactions between substrate-binding sites, each of the above steps can be treated as *pseudo*-first-order processes with the rate coefficients k_{obs1} and k_{obs2}, corresponding to the first and second steps, respectively (Fig. 2). Measurements of the specific rates of binding of DAPA to DTBS were determined over a DAPA concentration range of 10–500 μM, in the presence of Mg^{2+} (2 mM) and, later, with Mg^{2+} absent. Analysis of the spectrophotometric data, using a non-linear regression approach, allowed calculation of the DTBS–DAPA equilibrium dissociation constant. The plots of k_{obs1} against DAPA concentration were linear, conforming to the equation $k_{obs1}=k_1[DAPA]+k_{-1}$ both in the presence and absence of Mg^{2+}. In the presence of

Table 1. Details of data collection and processing.

DTBS data set	Resolution (Å)	Completeness (%)	I/σI	R_{merge} (%)	Multiplicity	Cell dimensions a	b	c	β	X-ray source (wavelength, Å)
Native	1.80	98.0 (92.3)	26.8 (8.0)	3.6 (10.9)	2.8 (2.7)	72.91	49.04	61.44	106.47	9.5 DL* 0.90
DAPA	2.37	86.0 (66.2)	14.7 (5.7)	10.6 (16.7)	3.0 (2.2)	73.21 +0.30	49.20 +0.16	61.31 −0.13	106.63 +0.16	7.2 DL* 1.488
N_2–DAPA–Mg^{2+}	2.30	99.1 (98.5)	21.9 (12.9)	6.1 (10.7)	3.7 (3.3)	73.00 +0.09	49.21 +0.17	61.13 −0.31	106.43 +0.04	7.2 DL* 1.488
CO_2–DAPA–Mg^{2+}	2.30	99.1 (95.1)	21.5 (11.3)	6.7 (13.3)	3.7 (3.2)	73.00 +0.09	49.21 +0.17	61.13 −0.31	106.43 +0.04	7.2 DL* 1.488

The numbers in brackets refer to the outer resolution shell. *DL refers to the SRS at the DRAL Daresbury Laboratory, UK, with the station number used also shown.

Table 2. The results of the refinements.

	Resolution (Å)	R (%)	Unique reflections	B model	Rms deviations bonds (Å)	angles (°)	dihedrals (°)	Cα (Å)
DAPA	10–2.33	15.7	7674	13.0	0.010 (0.01)	2.11 (0.5)	23.3(5.0)	0.167
N_2–DAPA–Mg^{2+}	10–2.30	15.4	8905	15.7	0.011 (0.01)	1.94 (0.5)	23.3 (5.0	0.285
CO_2–DAPA–Mg^{2+}	10–2.30	15.8	8932	17.7	0.010 (0.01)	1.93 (0.5)	23.3 (5.0)	0.276

All measured reflections were included in the refinements. The guide rms values are shown in parentheses. The last column shows the rms deviation of the positions of Cα atoms from those of the native structure.

Mg^{2+}, k_1=14.7 M^{-1} s^{-1} and k_{-1}=2.86×10^{-2} s^{-1}, giving a thermodynamic dissociation constant, K_{d1}, of 1.95 mM at 25°C. When these experiments were repeated in the absence of Mg^{2+}, the rate of DTBS–DAPA complex formation markedly decreased (k_1=0.63 M^{-1} s^{-1}) but the dissociation rate was virtually unchanged (k_{-1}=2.94×10^{-2} s^{-1}), giving a K_{d1} of 46.7 mM for the Mg^{2+}-free complex. Thus, Mg^{2+} accelerates the rate of formation of the DTBS–DAPA complex by an order of magnitude, but the dissociation rate of the Mg^{2+}-free enzyme–substrate complex is similar to that observed when Mg^{2+} is bound (Table 3).

Table 3. Kinetic data for DTBS.

	k_1($M^{-1}s^{-1}$)	k_{-1}(s^{-1})	K_{d1}(mM)	k_2($M^{-1}s^{-1}$)	k_{-2}(s^{-1})	K_{d2}(mM)
5 mM Mg^{2+}	14.7	0.026	1.95	4.82	0.25	51.0
No Mg^{2+}	0.63	0.029	46.7	–	–	–

Preliminary binding studies of crystals soaked in low concentrations of DAPA (0.2–5 mM), in the absence of Mg^{2+}, were consistent with this result [14]. Under these conditions DAPA binding was barely detectable and the only significant conformational change was the rotation of Tyr187, on helix α7, towards the positive pole of helix α6 and away from the pocket formed by helix α7 and the loop between strand β6 and helix α6. In crystals soaked at higher DAPA concentrations (20 mM, DAPA data set in Tables 1,2), the substrate orientation, together with the movement of Tyr187, is clearly visible in the difference electron density maps (F_{soak}–F_{nat}),Φ_{nat}, the phases being calculated from the native structure in the absence of DAPA (see Fig. 3a). Apart from the Tyr187 rotation, there was no significant change, from the unbound state, in the conformation of DTBS.

The k_{obs2} is linearly dependent upon the concentration of HCO_3^- (and by inference CO_2). At 25°C, with a DAPA concentration of 4 mM and a Mg^{2+} concentration of 2 mM, k_{obs2}=9.67×10^{-3} s^{-1} and k_2=4.82 M^{-1} s^{-1}. Simulation, using the kinetic model shown in the Figure 2, gave k_{-2}=0.25 s^{-1}, corresponding to a K_{d2} of around 51 mM for the DTBS–Mg^{2+}–DAPA.CO_2 complex. In contrast, in the absence of Mg^{2+}, no detectable reaction of the DTBS–DAPA complex with CO_2 could be observed. The kinetic results are summarized in the Table 3. It follows that neither binding of CO_2 to the enzyme, nor *N*-carboxylation, occurs to any significant extent in the absence of Mg^{2+}.

Binding of the carboxylate end of the substrate is invariant

In all complexes studied, the difference electron density maps (see Fig. 3) show unambiguously that the substrate and intermediate bind to the same site in the enzyme. Although the interactions at the diamino end of the substrate differ significantly in all enzyme–substrate complexes, the binding of the carboxyl group of the ligand is always the same. The carboxylate of DAPA (pK_a 4.48) interacts with the positive (N-terminal) pole of the helix

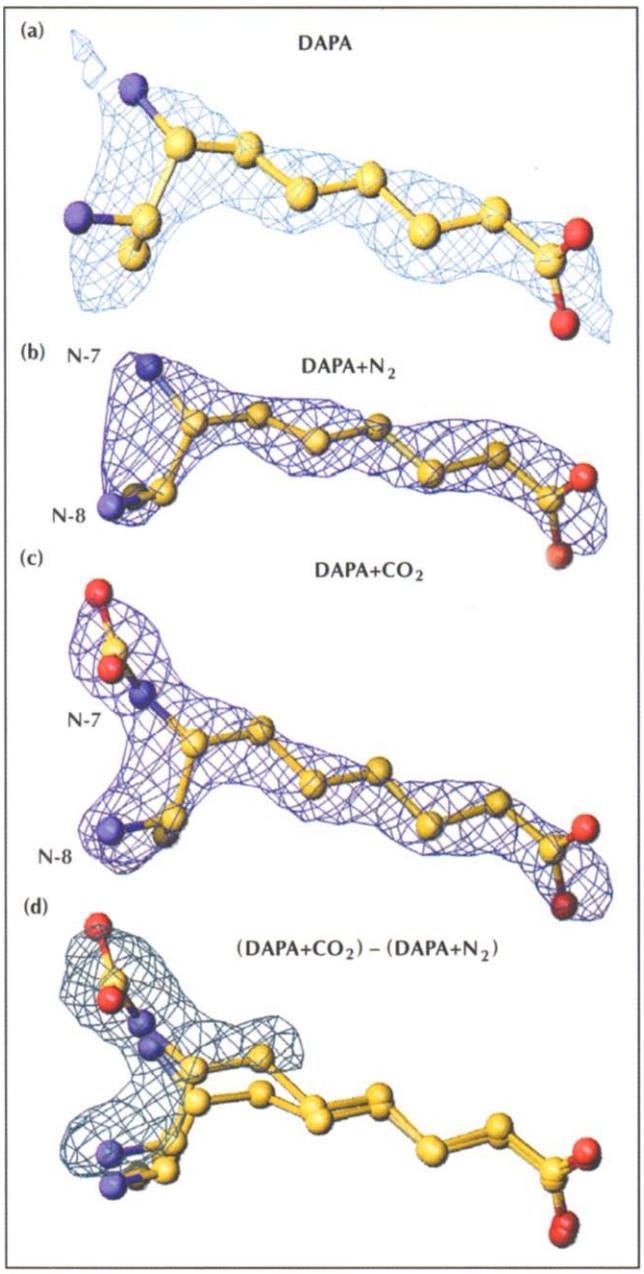

Fig. 3. The difference electron density maps (F_{soak}–F_{nat}),ϕ_{nat} contoured at the 3σ level. **(a)** The structure of DAPA in the Mg^{2+}-free complex. **(b)** DAPA bound to DTBS, in 20 mM $MgSO_4$ and in a CO_2-free nitrogen atmosphere. **(c)** The carboxylated substrate which is formed in a CO_2 atmosphere. **(d)** The difference electron density map (F_{CO_2}–F_{N_2}),ϕ_{N_2} shows that DAPA forms the N-7 rather than N-8 carbamate. Both DAPA and its carbamate are shown. (Yellow=carbon, red=oxygen and blue=nitrogen.)

α6 (see Fig. 4). One carboxylate oxygen binds to the main-chain nitrogen of Asn153 and the other is held between the positively polarized main-chain nitrogens of Gly150–Cys151–Ile152 and the hydroxyl of Tyr187, which moves to optimize substrate binding. Similar binding of the carboxylate of a substrate by a helix dipole is also observed in D-alanine-D-alanine ligase [16]. Tyr187, whose movement is clearly seen in all difference maps, is situated at the interface between the two monomers of the DTBS homodimer. In the native state, there is a hydrogen-bond to the hydroxyl group of Thr80 in the other subunit but on substrate binding this direct subunit–subunit interaction is lost.

The hydrophobic side chain of the bound DAPA lies in a groove on the other subunit. This surface is defined, in the native structure, by Cα of Gly118, Cγ2 of Thr122, Cα of Ser81 and Cδ of Pro82. In the DTBS–ligand complexes, the side chain of Leu149, which is in the carboxylate-binding subunit, moves some 2.5 Å towards the substrate, providing an additional hydrophobic interaction with the C3–C5 region of the polymethylene chain, that helps to lock the substrate in the groove of the opposite subunit (see Fig. 5c).

In contrast, the bonding pattern at the diamino end of the substrate is variable and subject to conformational changes of the enzyme, depending on the nature of the ligand and the presence of Mg^{2+} (see below), suggesting that the C-terminal end serves to anchor the substrate to the enzyme, presenting the diamino functionality to the catalytic site on the other subunit. The constraints imposed by the carboxylate-binding site and the hydrophobic trough suggest that alteration of the chain length of the substrate should lead to dramatic changes in binding. Indeed, shortening or lengthening the substrate chain by one CH_2 group results in an increase in K_{d1} of an order of magnitude (RL Baxter *et al.*, unpublished data).

Mg^{2+} induces conformational changes in the enzyme–DAPA complex

The coordination of the bound substrate in the absence of CO_2 but with Mg^{2+} present is shown in Figure 5a. The substrate is bound between the two crystallographically identical monomers of the dimeric DTBS. The N-8 amino group of DAPA is bound to the hydroxyl group of Thr11, situated on the flexible nucleotide-binding loop (P loop), and the N-7 amino group is hydrogen-bonded to the side-chain hydroxyl of Ser41, which projects from the rigid end of strand β3 [14]. These are the only direct hydrogen bonds formed between the enzyme and the amino groups of the substrate. In Figure 5, the arrow that represents strand β6 is drawn one residue shorter to show the backbone NH of Ser41 bound to the water molecule W2 (see below). In the absence of Mg^{2+}, the side-chain hydroxyl groups of Thr11 and Ser41 are too far apart for both to hydrogen-bond to DAPA when it is positioned between them. The conformational changes between the Mg^{2+}-bound and the Mg^{2+}-free substrate–enzyme complex are presented in Figure 5c. As the only pronounced difference between the conformation of the Mg^{2+}-free enzyme and its complex with DAPA is the rotation of the Tyr187 side chain, this figure also shows the conformational changes of the DAPA–DTBS complex that are induced by Mg^{2+} binding.

Without Mg^{2+}, the distance between the Cα atoms of Thr11 and Ser41 is 13.1 Å and the Thr11 and Ser41 hydroxyls are directed away from the substrate-binding

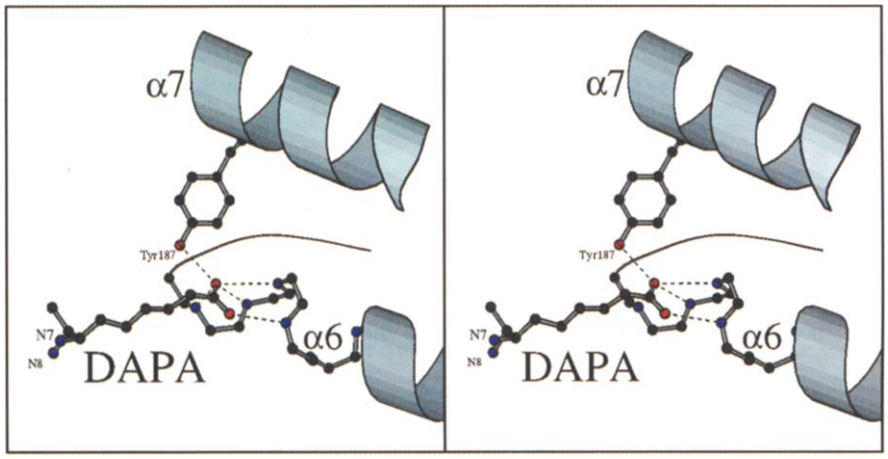

Fig. 4. The stabilization of the carboxylate end of the substrate bound to the positive pole of helix α6. The hydrogen-bonds shorter than 3.4 Å are shown by dotted lines. The figure was prepared using MOLSCRIPT [25].

site. Furthermore, the amino groups of the substrate are hydrogen bonded to the protein through water molecules (Fig. 5c, water molecules not shown); however, in the Mg^{2+}-bound complex, the Thr11–Ser41 Cα–Cα distance is shortened by 1.3 Å and both side-chain hydroxyl groups are rotated towards the binding site for the DAPA diamino group. The distance between the hydroxyl oxygens becomes 7.7 Å which allows hydrogen bonding of both hydroxyls with the substrate amino groups (Fig. 5c).

On the basis of earlier work on the Mg^{2+}-free DTBS–ADPNP complex, we suggested that the positions of the two bound sulfate ions, S1 and S2, from the crystallization medium could be considered to mimic the positions of the α- and γ-phosphates of the ATP molecule (for details see [14]). However, the intersulfate distance in the Mg^{2+}-free structure is too long to accommodate the ATP α- and γ-phosphates. In the presence of Mg^{2+}, the sulfates (Fig. 5c) are shifted about 0.8 Å, with respect to their positions in the absence of Mg^{2+}, towards the position of the active-site Mg^{2+} ion. The reduction of the intersulfate distance to 4.7 Å allows a better fit to the interphosphate distance for ATP. The P loop of the enzyme backbone follows the movement of the sulfates.

Thus, binding of Mg^{2+} to the enzyme leads to a movement of the P loop that has two consequences; the phosphate-binding site alters to permit better binding of the α- and γ-phosphates of ATP and the hydroxyl groups of Thr11 and Ser41 rotate towards the bound Mg^{2+}, and each other, allowing formation of hydrogen bonds between these residues and the amine groups of the substrate.

The N-7 amino group of DAPA is carboxylated and the N-7 carbamate oxygens replace the sulfate S2

There are two amino groups in the substrate, either of which could be a potential carboxylation site. The data sets N_2–DAPA–Mg^{2+} and CO_2–DAPA–Mg^{2+} were collected from a single crystal and show in detail where the carboxylation occurs. The data collected without and with CO_2 show that the conformation of the enzyme does not change; however, the difference electron density map $(F_{CO_2}–F_{N_2}),\phi_{N_2}$ shows one major maximum adjacent to the N-7 amino function which can only be interpreted in terms of carbamate formation at this position (Fig. 3d). This provides conclusive evidence that the DAPA N-7 carbamate is the enzyme-bound intermediate formed in this reaction.

The major negative peak (not shown) in the difference map $(F_{CO_2}–F_{N_2}),\phi_{N_2}$ covers the sulfate S2 which occupies the position of the putative γ-phosphate of ATP. The sulfate S2, which is present before DAPA carboxylation and which is coordinated to the Mg^{2+} ion, the ζ-amino groups of Lys37 and Lys15, and water molecule W2 (Fig. 5a, green), is removed and replaced by the carboxylate group of DAPA carbamate and the water molecule W1 (Fig. 5b, green). One of the oxygens of the carbamate (Fig. 5b) takes the position of water W2 in the non-carboxylated complex and coordinates to the ζ-amino group of Lys37. The other carbamate oxygen replaces one of the oxygens of the sulfate S2 and coordinates with the ζ-amino group of Lys37 and the water molecule W1, which takes the place of a second S2 oxygen. Small movements (up to 0.3 Å) of the Mg^{2+} ion, the sulfate anion S1, and the P loop, close the gap left by displacement of the S2 sulfate. The ζ-amino groups of Lys37 and Lys15 are now no longer linked through one of the S2 oxygens, Thr11 becomes coordinated to water W1 rather than to the N-8 amino group of the substrate, and W1 in turn forms hydrogen-bonds with the oxygen of the DAPA carbamate and the ζ-amino group of Lys15. The only direct contacts between the diamine-binding site and the carbamate are those with the ζ-amino group of Lys37 and the hydroxyl of Ser41.

The essential residues are conserved in DTBS sequences

There are now four published DTBS sequences (*E. coli* [3,11,15], *Bacillus sphaericus* [4], *Serratia marcescens* [SWISSPROT data bank, accession P36572] and *Brevibacterium flavum* [17]). CLUSTAL [18] was used to produce automatically an alignment which shows that the majority of the residues involved in the mechanism we propose here are conserved in these sequences. Perhaps the only surprising replacement is that of Tyr187, which is replaced by glutamine in the *B. sphaericus* sequence and by asparagine in the *B. flavum* sequence; however, it might

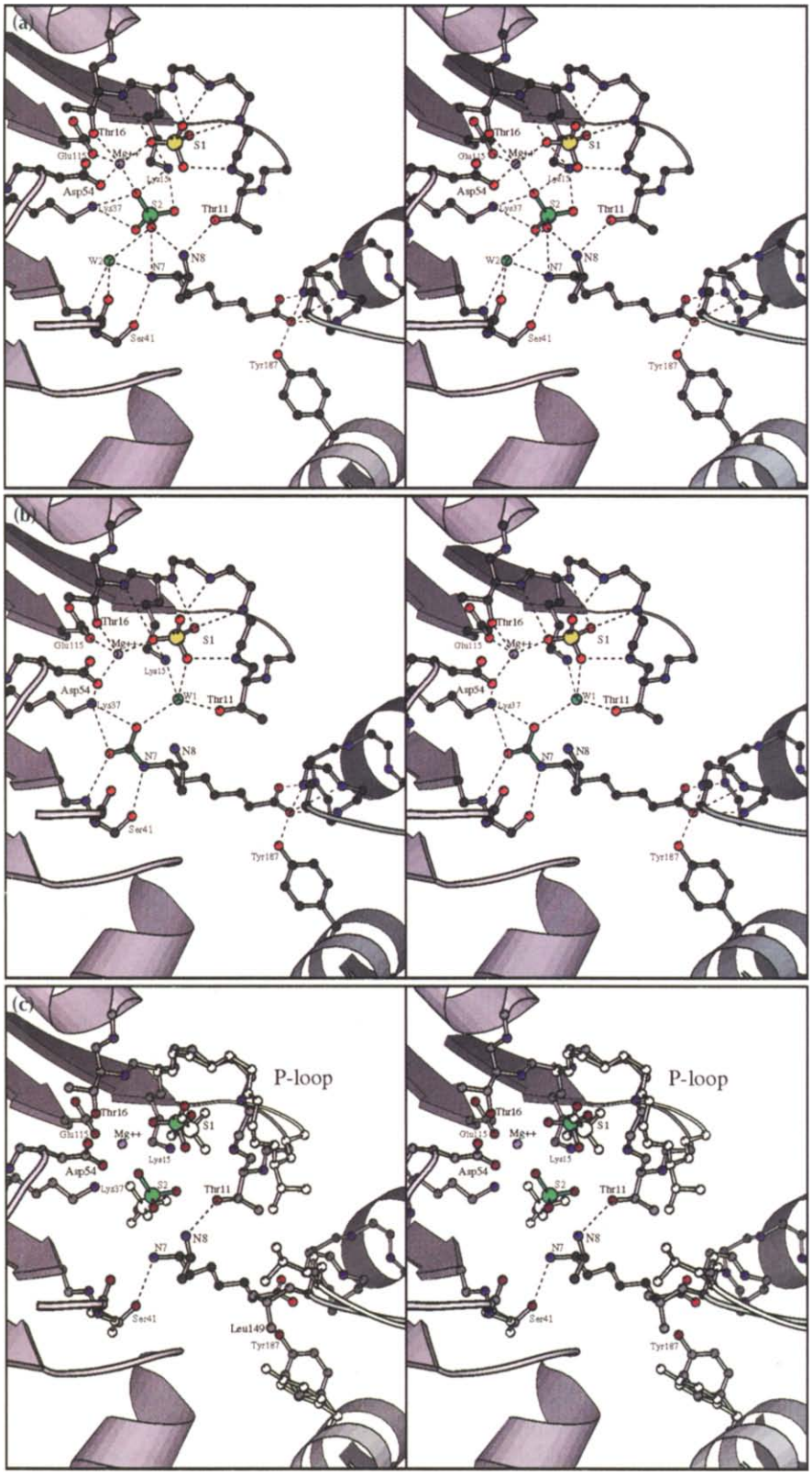

Fig. 5. Substrate binding to DTBS. **(a)** The substrate binding without CO_2, but with 20 mM Mg^{2+} present. S1 and S2 are the positions of the bound sulfate ions. **(b)** The carboxylated substrate with 20 mM Mg^{2+} present. The green colours in (a) and (b) highlight the differences between the carboxylated and non-carboxylated complexes. **(c)** The conformational changes induced by Mg^{2+} ions. The coloured molecule represents the Mg^{2+}-bound complex and the white molecule corresponds to Mg^{2+}-free enzyme. The hydrogen-bonds shorter than 3.4 Å are shown by dotted lines. The figure was prepared using MOLSCRIPT [25].

be noted that the side chains of both these residues are capable of forming hydrogen bonds. We would suggest, therefore, that it is not unlikely that the structures of these particular proteins could have a slightly differently oriented α7 helix, allowing these residues to stabilize DAPA carboxylate interaction with the protein.

The DTBS nucleotide-binding P loop is one residue longer than usual [14], and this feature is conserved in all four DTBS sequences. The elongation can be explained in terms of the substrate binding. The small bulge in the middle of the loop is occupied by Thr11, which is hydrogen-bonded to the N-8 amine of the substrate.

This interaction is essential for the correct orientation of the N-7 amine to allow carboxylation. Thus, the elongated P loop can simultaneously bind both ATP and substrate, which brings them together in order to facilitate carbamate phosphorylation. We suggest that the dual function of an elongated P loop may be of mechanistic significance in other enzymes [14].

Mechanism of DTBS

The detail revealed in these experiments enables us to formulate a reasonable mechanistic proposal for the roles played by Mg^{2+}, DAPA, ATP and the residues of the enzyme active site, in the sequence of reactions catalyzed by DTBS. The binding of the substrate to the enzyme does not require ATP but is strongly influenced by the presence of Mg^{2+}. In the absence of Mg^{2+} the only direct interactions between DAPA and DTBS are those of the DAPA carboxylate with the positive pole of the α6 helix and the phenolic hydroxyl of Tyr187. In this complex, the amino end of DAPA appears to be loosely hydrogen bonded to DTBS, through bound water. It is noteworthy that no measurable reaction of the substrate with CO_2 occurs in the Mg^{2+}-free complex.

Mg^{2+} binding induces a sequence of structural changes in the DAPA-binding site of DTBS, represented pictorially in Fig. 5c, which result in a 20-fold reduction in the dissociation constant of the enzyme–substrate complex. This equates to a ΔG^{o}, for DTBS–Mg^{2+}–DAPA complex formation of −15.5 kJ mol^{-1}, compared with −7.5 kJ mol^{-1} for the DTBS–DAPA complex in the absence of Mg^{2+}. Essentially, the major structural changes that are responsible for this, and are described in detail above, are the formation of hydrogen bonds between the hydroxyls of Ser41 and Thr11 and the N-7 and N-8 amino groups of the substrate. The geometry of the DTBS–Mg^{2+}–DAPA complex forces distinction of the two amino groups, and it is clear from the structure of the carbamate complex that the N-7 amino group acts as a nucleophile in the carboxylation reaction. In the crystallographic DTBS–Mg^{2+}–DAPA complex, the N-7 amino group is close to the bound S2 sulfate which suggests that this sulfate may play a role in proton abstraction, making the amino group susceptible to electrophilic attack. Comparison with our preliminary results [15], and unpublished work on the DTBS–ADPNP complex, suggests that the S2 sulfate of this structure occupies virtually the same site as the γ-phosphate group of ATP (which is required in a subsequent step). On this basis, we conjecture that under catalytic conditions the ATP γ-phosphate group, instead of the sulfate, could play a role in proton abstraction.

Reaction of the DTBS–Mg^{2+}–DAPA complex with CO_2 results in formation of the bound DAPA carbamate complex. The formation of the DAPA carbamate (Fig. 5b) results in displacement of the S2 sulfate from the complex, although no significant movement of the DAPA backbone is involved (Fig. 3d). This suggests that in the carboxylation transition state the incoming CO_2 may be polarised by the protonated ζ-amino group of Lys37, increasing the δ+ nature of the carbon and potentiating nucleophilic attack by N-7.

Following the reasoning that the binding of the S2 sulfate in the DTBS–Mg^{2+}–DAPA complex merely mimics that of the γ-phosphate of ATP, it seems likely that under catalytic conditions, when ATP is present (K_m 19 μM), the S1 and S2 sites are normally occupied by the ATP α- and γ-phosphates. This view is supported by the results of steady-state kinetic measurements in the presence of ATP, that show a K_m for DAPA of 3 μM, contrasting dramatically with the K_{d1} value of around 2 mM for the DTBS–Mg^{2+}–DAPA complex measured in the absence of ATP. The displacement of S2 that occurs during the conversion of DTBS–Mg^{2+}–DAPA complex to the bound carbamate complex also suggests that, when ATP is bound, carbamate formation results in displacement of the γ-phosphate of ATP from the S2 site. This would have the effect of increasing the δ+ nature of the phosphorus atom of the γ-phosphate, increasing its vulnerability to nucleophilic attack. Thus, under normal steady state conditions, the subsequent carbamate phosphorylation (step 5 in Fig. 1) might be expected to occur virtually spontaneously.

Biological implications

Dethiobiotin synthetase (DTBS) is an unique ATP-dependent carboxylase that catalyzes the insertion of CO, derived from carbon dioxide, between the vicinal amino groups of the substrate, (7*R*,8*S*) 7,8-diaminononanoic acid (DAPA), eventually resulting in formation of the *ureido* ring of dethiobiotin (DTB), the immediate precursor of the vitamin biotin. DTBS is one of the few carboxylation enzymes that has been characterized that uses CO_2, rather than hydrogen carbonate, as a substrate. Apart from its use of CO_2, DTBS appears to bear no mechanistic similarity with C-carboxylating enzymes such as ribulose-1,5-bisphosphate carboxylase/oxidase and phosphoenolpyruvate carboxykinase. DTBS, which is active as a homodimer, has structural similarities to several other enzymes that utilize nucleotide triphosphates, notably nitrogen Fe protein and adenylosuccinate synthetase. These proteins also have an elongated P loop.

The structural changes involved in the formation of the DTBS–Mg^{2+}–DAPA (substrate) and DTBS–Mg^{2+}–DAPA.CO_2 (carbamate intermediate) complexes, in conjunction with solution kinetic measurements, suggest a mechanistic model in which binding of Mg^{2+} and the triphosphate element of ATP (which can be mimicked by sulfate) to DTBS creates the appropriate geometry for substrate DAPA-binding and carbamate formation. Further studies using intermediate analogs and rationally designed DTBS single residue mutants are required to probe the detailed interactions involved in the reaction sequence.

Materials and methods

Crystallography

Crystals of DTBS were grown from ammonium sulfate as previously described [11]. Buffers and salts were purchased from Sigma Chemicals plc, Poole, Dorset, England.

For the substrate soaking experiments the native enzyme crystals were grown without Mg^{2+} and the substrate and/or $MgSO_4$ were dissolved in the crystallization well solution. Several crystals of typical dimensions $0.15\times0.15\times0.15$ mm^3 were then added to this solution and equilibrated for time periods of 20 minutes to overnight. The equilibration time did not affect the substrate binding and the crystals did not deteriorate during soaking. The 20 mM substrate was soaked into the crystal overnight in the absence of Mg^{2+} and collected in the ambient atmosphere (data set DAPA). Another data set was collected from a crystal soaked in 100 mM DAPA in the presence of 20 mM $MgSO_4$. Before data collection the soaked crystal was equilibrated in an N_2 atmosphere for 4 h to remove atmospheric CO_2 (data set N_2-DAPA-Mg^{2+}). After the data were collected, the atmosphere around the crystal was purged with CO_2 and the crystal was left to equilibrate for a further 2 h. A second data set was then collected from this same crystal (data set CO_2-DAPA-Mg^{2+}). The overall temperature factor rose from 10.0 Å^2 for the first set of data to 16.0 Å^2 for the second; the R factor between the data sets was 8.9%.

The native data were collected and processed as already described [14]. X-ray data for the substrate-soaked crystals were collected on station 7.2 at the SRS, Daresbury Laboratory, at a wavelength of 1.488 Å using an 18 cm MAR image plate system. The crystals were cooled to 260 K to increase the crystal lifetime. Data were processed with DENZO [19] and the CCP4 Suite of programs [20]. Refinement was carried out with the program X-PLOR [21] and the models examined with the program 'O' running on a Silicon Graphics Indigo II workstation [22].

The difference Fourier maps $(F_{soak}-F_{nat})$,ϕ_{nat}, with phases calculated from the native protein (Fig. 3b,c) are contoured at the 3σ level with the maximum of about 9σ in all 3 cases. The models for DAPA were built into the difference density and the structures were independently refined (see Table 2). The native enzyme (224 amino acids, 1692 non-hydrogen atoms) was used as the starting model in each case. Simulated annealing at 4000 K was followed by positional refinement; the water molecules were found and refined automatically with the program ARP [23] for all structures, and were all checked by molecular graphics to ensure that they made chemical sense. There were 221 of them in the case of N_2–DAPA–Mg^{2+}, 223 in case of CO_2–DAPA–Mg^{2+} and 209 for DAPA. The positions of most of them are common to all structures. The position of the Mg^{2+} ion, closely coordinated between the hydroxyl of Asp54 and two sulfate ions, was clearly visible in the electron density maps $(3|F_{obs}|-2|F_{calc}|)$,ϕ_{calc}. The ion was introduced into the structure and the coordination distances were found to be about 2.2 Å after refinement. The occupancies of all protein atoms were fixed and the occupancies of the ligand, Mg^{2+} ion and the water molecules, were refined. The occupancy of the substrate in the refined models was 0.9 for the Mg^{2+}-free structure and 1.0 for two other structures with Mg^{2+}. Finally, the isotropic restrained B-factor refinement converged to R factors of about 16% (see Table 2).

The major feature in the difference map $(|F_{CO_2}|-|F_{N_2}|)$,ϕ_{N_2} calculated using the phases from the structure N_2–DAPA–Mg^{2+} unambiguously showed the position of the CO_2 molecule bound to DAPA and agreed with the results of the refinement (Fig. 3d). This map is contoured at the 3σ level. Another difference Fourier map with coefficients $(|F_{CO_2}|-|F_{N_2}|)$ but calculated with phases ϕ_{nat}, from the native model, showed the same features. The only major negative peak in both difference maps is about 10σ and covers the sulfate S2 indicating that this sulfate is present in the CO_2-free crystal and is removed as the result of carboxylation.

As an independent check on the position of the carbamate, a difference Patterson synthesis with coefficients $(|F_{CO_2}|-|F_{N_2}|)^2$ was calculated. It shows a single major positive peak of 8σ on the Harker sections, which is consistent with the position of the sulfate S2 in the CO_2-free structure. The (x,z) coordinates of the sulfate S2 are x=27.6, z=16.0 Å and the coordinates of the corresponding peak at the Harker section y=0 (the space group is C2) are 2x=55.8, 2z=32.2 Å, which is within 0.3 Å of the expected position. This peak directly indicates that the sulfate is removed as the result of carboxylation.

The model building and refinement of the models for N_2–DAPA–Mg^{2+} and CO_2–DAPA–Mg^{2+} was straightforward and gave good quality difference maps $(3F_{obs}-2F_{cal})$,ϕ_{cal} that clearly showed the carboxylation of the substrate. The difference maps $(|F_{DAPA}|-|F_{N_2}|)$,ϕ_{N_2}, $(|F_{DAPA}|-|F_{CO_2}|)$,ϕ_{CO_2} and $(|F_{DAPA}|-|F_{nat}|)$,ϕ_{nat} were also inspected at both positive and negative levels, using O, on a Silicon Graphics workstation.

In the Mg^{2+}-free case (data set DAPA), binding at the amino end of DAPA was less clear cut. The positive density in the map $(|F_{DAPA}|-|F_{nat}|)$,ϕ_{nat}, with phases from the Mg^{2+}-free native crystal structure without substrate, clearly showed DAPA in the same position as for the Mg^{2+}-bound complexes (not shown). The major negative peak in the map covered the position of sulfate S2, indicating that S2 is displaced from the substrate-bound complex. This negative peak is also the major negative feature of the map $(|F_{DAPA}|-|F_{N_2}|)$,ϕ_{N_2} constructed with phases from the structure equilibrated in the CO_2-free, N_2 atmosphere with 20 mM $MgSO_4$. Sulfate S2 is replaced by CO_2 in the DTBS–Mg^{2+}–DAPA.CO_2, complex, and consequently, the map $(|F_{DAPA}|-|F_{CO_2}|)$,ϕ_{CO_2} should have significant positive density at the S2 position if S2 was present in the DAPA complex (it is absent in the DTBS–Mg^{2+}–DAPA.CO_2 complex). Inspection of these three difference maps leads to the conclusion that sulfate S2 is absent in the Mg-free, substrate bound crystal, present in the DAPA–Mg^{2+} complex, and is substituted by the CO_2 molecule. However the maps $(3F_{obs}-2F_{cal})$,ϕ_{cal} and $(F_{obs}-F_{cal})$,ϕ_{cal} for the CO_2-bound model showed significant traces of the sulfate electron density. The partial CO_2/S2 model agrees well with the maps implying that CO_2 and S2 compete for the same binding site.

Kinetic measurements

UV measurements were carried out using a Hewlett Packard 8452A Diode Array Spectrophotometer with a SFA-20 Rapid Kinetics Stopped-Flow Accessory (Hi-Tech Scientific Ltd., Salisbury, UK). Reaction temperatures were maintained with the use of a RTE-100 circulatory water bath (NESLAB Instruments Inc., Newington, NH). Measurements were made at 25°C (±0.1°C) in 0.1 M tris buffer containing 50 mM KCl, 0.2 mM EDTA, 0.5 mM 2-mercaptoethanol (and 2 mM $MgCl_2$) adjusted to pH 7.8 at 25°C with enzyme concentrations of 0.5–1.0 mM. Data were collected using a HP Vectra VL2 4/50 computer and analyzed on line using various software products (HP 89532A General Scanning Software, HP

89532K UV-Visible Kinetics Software and SPECFIT v2.0, Spectrum Software Associates, Chapel Hill, NC). The coefficients k_{obs}, k_{obs1} and k_{obs2} were determined using non-linear regression by a combination of the Levenberg-Marquardt algorithm and the simplex method [24]. Values of k_1, k_{-1} and k_2 were obtained from k_{obs}/[substrate] plots. k_{-2} was estimated by fitting the kinetic model (see Fig. 2) to time-dependent absorption changes in the 200–400 nm range using experimental values for k_1, k_{-1} and k_2 and initial conditions [DAPA]=4 mM, [DTBS]=60 mM, [CO_2]=2 mM, and [DTBS–Mg^{2+}–DAPA]=[DTBS–Mg^{2+}-DAPA.CO_2]=0.

The coordinates for the structures referred to in Table 1 have been deposited at the Brookhaven Protein Databank.

Note added in proof

The attention of the reader is drawn to two recent papers from DuPont and Uppsala *(Biochemistry* [1995], **34**: 10976–10984 and 10985–10995, respectively) which confirm the involvement of N-7 rather than N-8. However, the involvement of Mg^{2+} in DAPA binding is not discussed.

Acknowledgements: We are grateful to BBSRC for financial support for this work. We are also indebted to the staff at DRAL Daresbury Laboratory for use of the SRS.

References

1. Fersht, A.R. (1985). *Structure and Mechanism of Enzymes*, W.H. Freeman, New York.
2. Cleary, P.P., Campbell, A. & Chang, R. (1972). Location of promoter and operator sites in the biotin gene cluster of *Escherichia coli*. *Proc. Natl. Acad. Sci. USA* **69**, 2219–2223.
3. Otsuka, A.J., *et al.*, & Matsuzaki, J. (1988). The *Escherichia coli* biotin biosynthetic enzyme sequences predicted from the the nucleotide sequence of the *bio* operon. *J. Biol. Chem.* **263**, 19577–19885.
4. Gloeckler, R., *et al.*, & Lemoine, Y. (1990). Cloning and characterisation of the *Bacillus sphaericus* genes controlling the bioconversion of pimelate into dethiobiotin. *Gene* **87**, 63–70.
5. Eisenberg, M.A. (1987). Biosynthesis of biotin and lipoic acid. In *Escherichia coli and Salmonella typhimurium: cellular and molecular biology* vol. 2. (Neeidhardt, F.C., ed), pp. 544–550, American Society for Microbiology, Washington, USA.
6. Baldet, P., Gerbling, H., Axiotis, S. & Douce, R. (1993). Biotin biosynthesis in higher plants. *Eur. J. Biochem.* **217**, 479–485.
7. Krell, M. & Eisenberg, M.A. (1970). The purification and properties of dethiobiotin synthetase. *J. Biol. Chem.* **245**, 6558–6566.
8. Eisenberg, M.A. & Krell, M. (1979). Dethiobiotin synthetase. *Methods Enzymol.* **62D**, 348–352.
9. Walsh, C. (1979). *Enzymatic Reaction Mechanisms*, W.H. Freeman, New York.
10. Hartman, F.C., & Harpel, M.R. (1994). Structure, function, regulation and assembly of D-ribulose-1,5-bisphosphate carboxylase/oxidase. *Ann. Rev. Biochem.* **63**, 197–234.
11. Alexeev, D., *et al.*, & Baxter, R.L. (1994). Sequence and crystallisation of *Escherichia coli* dethiobiotin synthetase, the penultimate enzyme of biotin biosynthesis. *J. Mol. Biol.* **235**, 774–776.
12. Baxter, R.L., Ramsey, A.J., McIver, L.A. & Baxter H.C. (1994). Mechanism of dethiobiotin synthetase — characterisation of the 8-aminocarbamate of (7*R*,8*S*) 7,8 diaminononanoate as an enzyme-bound intermediate. *J. Chem. Soc., Chem. Commun.* 559–560.
13. Baxter, R.L. & Baxter, H.C. (1994). Mechanism of *Escherichia coli* dethiobiotin synthetase — closure of the *ureido* ring of dethiobiotin involves formation of a carbamicphosphate mixed anhydride. *J. Chem. Soc., Chem. Commun.* 759–760.
14. Alexeev, D., Baxter, R.L. & Sawyer, L. (1994). Mechanistic implications and family relationships from the structure of dethiobiotin synthetase. *Structure* **2**, 1061–1072.
15. Huang, W., Lindqvist, Y., Schneider, G., Gibson, K.J., Flint, D. & Lorimer, G. (1994). Crystal structure of an ATP-dependent carboxylase, dethiobiotin synthetase, at 1.65 Å resolution. *Structure* **2**, 407–414.
16. Fan, C., Moews, P.C., Walsh, C.T. & Knox, J.R. (1994). Vancomycin resistance: structure of D-alanine-D-alanine ligase at 2.3 Å resolution. *Science* **266**, 439–443.
17. Hatakeyama, K., Hohama, K., Vertes, A.A., Kobayashi, M., Kurusu, Y. & Yukawa, H. (1994). Genomic organisation of the biotin biosynthetic genes of corneform bacteria: cloning and sequencing of the *bioA-bioD* genes from *Brevibacterium flavum*. *DNA Sequence* **4**, 177–184.
18. Higgins, D., Bleasby, A.J. & Fuchs, R. (1994). CLUSTAL-V — Improved software for multiple sequence alignment. *Scientist* **8**, 17–21.
19. Otwinowski, Z. (1988). *DENZO. A program for automatic evaluation of film densities.* Department of Molecular Biophysics and Biochemistry, Yale University, New Haven, CT.
20. Collaborative Computational Project No. 4 (1994). The CCP4 Suite: Programs for Protein Crystallography. *Acta Cryst. D* **50**, 760–763.
21. Brünger, A.T. & Krukowski, A. (1990). Slow-cooling protocols for crystallographic refinement by simulated annealing. *Acta Cryst. A* **46**, 585–593.
22. Jones, T.A., Zou, J.Y., Cowan, S.W. & Kjeldgaard, M. (1991). Improved methods for building protein models in electron density maps and the location of errors in these models. *Acta Cryst. A* **47**,110–119.
23. Lamzin, V.S. & Wilson, K.S. (1993). Automatic refinement of protein models. *Acta Cryst. D* **49**,129–147.
24. Gampp, H., Maeder, M., Meyer, C.J. & Zuberbuhler, A.D. (1985). Calculation of equilibrium-constants from multiwavelength spectroscopic data. 2. SPECIFIT — 2 user-friendly programs in basic and standard FORTRAN-77. *Talanta* **32**, 257–264.
25. Kraulis, P.J. (1991). MOLSCRIPT: a program to produce both detailed and schematic plots of protein structure. *J. Appl. Cryst.* **24**, 946–950.

Received: **25 Jul 1995**; revisions requested: **21 Aug 1995**; revisions received: **29 Aug 1995**. Accepted: **5 Sep 1995**.